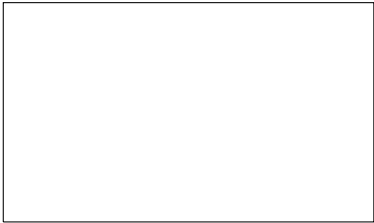


Graphical Abstract

This is a specimen a_b title

J.K. Krishnan, Han Thane, William J. Hansen, T. Rafeeq



Highlights

This is a specimen a_b title

J.K. Krishnan, Han Thane, William J. Hansen, T. Rafeeq

- Research highlights item 1
- Research highlights item 2
- Research highlights item 3

This is a specimen a_b title^{*,**}

Sir J.K. Krishnan^{a,c,*,1} (Researcher), Han Thane^{b,d}, William J. Hansen Jr^{b,c,2} (Co-ordinator) and T. Rafeeq^{a,c,**,1,3}

^aDepartment of Physics, J.K. Institute of Science, Jawahar Nagar, Trivandrum, 695013, Kerala, India

^bWorld Scientific University, Street 29, 1011 NX Amsterdam, The Netherlands

^cUniversity of Intelligent Studies, Street 15, Jabaladesh, 825001, Orissa, India

ARTICLE INFO

Keywords:

quadrupole exciton

polariton

WGM

BEC

ABSTRACT

The advancement and ubiquity of digital networks have fundamentally transformed numerous spheres of human activity. At the heart of this phenomenon, lies the Transmission Control Protocol (TCP) model, whose influence is particularly notable in the exponential growth of the Internet due to its ability to transmit flexibly to any device, through its advanced Congestion Control (CC). Seeking an even more efficient CC mechanism, this work proposes the construction of deep learning neural networks (MLP, LSTM, and CNN) for classifying the level of network congestion. The results attest to models capable of distinguishing, with over 90% accuracy, between moments of high and low degrees of congestion. With this, it becomes possible to differentiate between congestion and random losses, potentially increasing throughput by up to five times in environments with random losses when combined with CC algorithms.

`\beginabstract ... \endabstract` and `\begin{keyword} ... \end{keyword}` which contain the abstract and keywords respectively. Each keyword shall be separated by a `\sep` command.

1. Introduction

Digital networks, fundamental to the daily lives of modern society, are widely governed by the TCP transport layer. This predominance derives from the broad range of services available on the internet, accessible through a variety of terminals with different architectures. The internet, which has quickly become accessible to around 95% of the global population ITU (2023), operates on a set of rules established by the TCP protocol. Such rules, embedded in operating systems, facilitate the application's data exchange through a series of layered structured services, known collectively as the TCP/IP protocol stack.

A critical element of this stack is the Transport Layer, carried out by Congestion Control (CC). CC is essential to TCP transmissions, adjusting how much data it should transfer in each transmission cycle. A crucial part of CC is the estimation of network congestion level, which, in most available implementations, is performed through losses that have already occurred or variations in delay during data exchange.

In this context, Deep Learning Networks, such as Multilayer Perceptron (MLP) Lippmann (1987), Long Short-Term Memory (LSTM) Hochreiter and Schmidhuber (1997), or Convolutional Neural Network (CNN) Fukushima (1980) emerge as architectures with promising methods for accurately estimating the level of congestion, before infrastructure saturation.


* This document is the results of the research project funded by the National Science Foundation.


** The second title footnote which is a longer text matter to fill through the whole text width and overflow into another line in the footnotes area of the first page.

This note has no numbers. In this work we demonstrate a_b the formation Y_1 of a new type of polariton on the interface between a cuprous oxide slab and a polystyrene micro-sphere placed on the slab.

*Corresponding author

**Principal corresponding author

 jkk@example.in (J.K. Krishnan); wjh@example.org (W. J. Hansen); t.rafeeq@example.in (T. Rafeeq)

 www.jkkkrishnan.in (J.K. Krishnan); <https://www.university.org> (W. J. Hansen); www.campus.in (T. Rafeeq)

ORCID(s): 0000-0001-0000-0000 (J.K. Krishnan)

¹This is the first author footnote, but is common to third author as well.

²Another author footnote, this is a very long footnote and it should be a really long footnote. But this footnote is not yet sufficiently long enough to make two lines of footnote text.

1.1. Research questions

Given the above, this work investigates the performance of these AI architectures, directly used in CC, seeking to answer the following research questions (RQ):

- **QP1: (Congestion Learning by Neural Networks)** Investigate the ability of a neural network to learn to classify the degree of congestion in a network connection, based on the occupancy of an output *buffer* in a topology *dumbbell*, present in most Internet connections.
 - **QP1.1: (Tolerance to Variation in the Number of Flows)** Evaluate whether the learning model is capable of maintaining its accuracy and effectiveness even when there are significant variations in the volume of traffic (flow) on the network.
 - **QP1.2: (Applicability to Various CC Mechanisms)** Determine whether the learned model can be effectively applied to flows that are controlled by different types of CC mechanisms.
- **QP2: (Identification of the Optimal Dimension for Congestion Classifiers)** Define the ideal combination of measures (such as data components and dimensions) to develop congestion classifiers that are both efficient and accurate.
- **QP3: (Gains from Learning in Random Loss Scenarios)** Examine whether a model developed from a neural network, trained with low-dimensional vectors, can lead to better use of available bandwidth, especially in scenarios characterized by random packet losses.

Based on the research questions outlined, we carried out a broad study through package-level simulations using ns-3 ns3 (2023). The flexibility of ns-3 allows you to explore different versions of TCP, machine learning models and number of flows (up to 40). The simulation results revealed effective performance of neural networks in detecting congestion levels.

This effectiveness also served to apply these models in a practical case: the distinction between random packet losses, a common phenomenon in wireless networks, including Wi-Fi connections and 4G and 5G cellular networks, showing the usefulness of the mechanism with significant improvement in transmission performance in these challenging conditions. To validate our results, we resorted to the use of a specific analytical equation for CC in loss scenarios, proving that the performance of competing protocols is negatively affected in the simulation, according to the literature.

2. Data Mining

To build a training dataset, we implemented a ns3 Traffic Analyzer (AT). The AT performs several simulations of a *dumbbell* topology (Figure 1), a common configuration in network research, which has a central bottleneck and several independent access links. The channels of the stations connected to Router 01 have 2ms delay. In all others, this time is 10ms. The transmission rate is 1Gbps on all channels, with the exception of the one between routers, the bottleneck, which is set to 10, 100, 500 and 1000 Mbps, according to the interested scenarios.

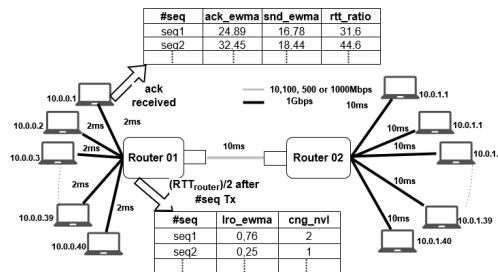


Figure 1: Topology used to acquire training, validation and tests data and for CC mechanisms evaluation..

Through the dumbbell topology, distributed TCP connections are established. Applications are on terminals connected to Router 01 and TCP servers are on those connected to Router 02. Router 01 10.0.0.2 Terminal connects to

terminal 10.1.0.2 of Router 02. Likewise, terminal 10.0.2.2 with the 10.1.2.2; 10.0.3.2 with 10.1.3.2 and so on, until - in case of 80 connections - the last connection, between stations 10.0.79.2 and 10.1.79.2.

The beginning of the connections are spaced of 0.5s to avoid synchronization. Terminal applications were configured to schedule data sending whenever there is space in the *socket* transmission queue. Once such space was identified, each application waits a random time interval t , $0 \leq t < 70$ to exhaust that queue again. This interval was chosen to maintain flows intensity and, at the same time, to make the simulations more realistic in terms of data send randomness.

The training data, for each bottleneck datarate, came from 60 Vegas TCP P2P flow, established on independent links, transporting data capable of saturating the bottleneck, during a 1.5-minute ns-3 simulations³. The AT generate two “.csv” files per flow. In the first, the following parameters, inspired by Remmy, are recorded for every ACK received by the sender:

- *#seq*: Sequence number, present in the ACK packet.
- *ack_ewma*: Weighted exponential moving average of arrival time between ACK packets.
- *snd_ewma*: Weighted exponential moving average of the interval between the timestamps present in the respective ACK.
- *rtt_ratio*: Dividing RTT by RTT_{min} .

To update the second .csv file, whenever a segment is sent in time t , the AT schedules an event at $t + RTT_{router}/2$, where RTT_{router} is the expected RTT between the transmitter and the edge router. During the event handling, the learning target parameters are recorded:

- *#seq*: Number of seq present in the segment for which the event was scheduled.
- *lro_ewma*: Weighted exponential moving average of the occupation percentage of the *buffer* of the edge router, to which the transmitter is connected (Router 01 in Figure 1).
- *cng_nvl*: Network congestion level. If $lro_ewma \leq 40\%$, $cng_nvl = 1$ or $cng_nvl = 2$, case $lro_ewma \geq 70\%$.

All moving averages were calculated in microseconds (μs), with a weight of 0.8 for new measurements, in order to prioritize the network momentary state. For training accuracy, the analyzer was configured to record when $lro_ewma \leq 40\%$ or $lro_ewma \geq 70\%$ only. This design seeks robust models in extreme situations, in case of underutilization or overload.

3. Data Processing

The data generated by the (AT) goes through the following stages, before forming the input vectors for the neural networks:

1. *Inner Join (IJ)*: The first step consists of generating a table that associates the *ack_ewma*, *snd_ewma* and *rtt_ratio* measurements, with *lro_ewma* and *cng_nvl*, through the *#seq* columns, present in both files collected by the AT.
2. *Redundancy Elimination (RE)*: Lines with identical *ack_ewma*, *snd_ewma* and *rtt_ratio* are discarded, keeping the last record throughout the simulation.
3. *Label Balancing (LB)*: The number of Records with $cng_nvl = 1$ must be the same as those with $cng_nvl = 2$. Excess data is disregarded.
4. *Attenuators Cut (AC)*: Records with *ack_ewma*, *snd_ewma* and *rtt_ratio* above the ninetieth percentile (P_{90}) are ignored.
5. *Input Normalization (IN)*: Each of the columns goes through a normalization process, in which its measurements are divided by the maximum value present in it. The normalizers collected from the training data will later be used in all other data that enter the constructed models.

³For 10Mbps bottleneck, we execute 11 simulations to take sufficient low congestion data.

Table 1
Neural networks Configuration

epoch:3000; batch size 64; learning rate: 0.0001		
MLP	LSTM	CNN
-Input: 3 dimensional vectors. -Layers: 3 (20 RELU). -Output: Sigmoid.	-Input: Matrix 3x3. -Layers: 2 (each one with 3 LSTM - 30% dropout). -Output: Sigmoid.	-Input: Image Vectors 3X3@1. -Convolution:16 maps - 1x3 -Stride: [1,1] -Convolution Output: RELU -Pooling: <i>maxpooling</i> , [1,2]. -Flattening: 64 RELU inputs. -Output: Sigmoid.

The resulting table is used to construct a set X , where each element x_i is a vector with components *ack_ewma*, *snd_ewma*, *rtt_ratio* properly treated. Each x_i receives a class $y_i \in Y = \{0, 1\}$, equal to 0 or 1, according to the value of *cng_nvl*. After the mentioned steps, we reached a set X of 20,000 entries, for each training process, executed per bottleneck datarate cenario.

4. Training Neural Networks - Obtaining the Models

4.1. Overview

The research attained its objectives using twelve models, varying the ARN (MLP, LSTM, CNN), whose specifications are in Table 1, associated with a combination of components (*ack_ewma*, *snd_ewma*, *rtt_ratio*). The type of neural network and the respective input vector components label each model. MLP₁₂₃, for example, refers to the model obtained by the MLP network, receiving the three components as input. LSTM₁₃ means model obtained by the LSTM neural network, receiving as input (*ack_ewma*, *rtt_ratio*); CNN₂₃ to CNN, which receives (*snd_ewma*, *rtt_ratio*).

Accuracy, Error, Precision, Recall, and F1, obtained from the *Receiver operating characteristics* (ROC) analysis⁴, will be used to compare the models extracted from learning networks. The ROC space is constructed from a Cartesian plane, with the abscissa and ordering associated, respectively, with the rates of false positives, or *False Positive Rate* (FPR), and true positives, or *True Positive Rate* (TPR), for a data set offered to the model.

4.2. Training Vector Transformations

For each of the ARNs, there was a need to transform the vectors from the set X . Transformations description uses three-dimensional vectors, with the components *ack_ewma*, *snd_ewma*, and *rtt_ratio*, as it is analogous to those with one or two components. Regarding MLP, for example, the transformation was direct, without more elaborated rearrangement (Figure 2a).

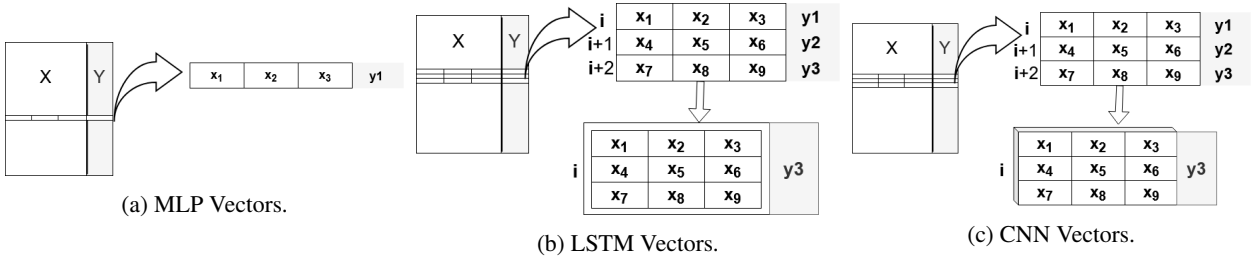


Figure 2: NNA data transformations.

The ARN based on LSTM and CNN required elaborate transformations. In LSTM, considering that X has m elements, each element x_i ($i + 2 \leq m$), accompanied by two consecutive vectors, will give rise to an entry in the LSTM network, associated with the class of the third sequence vector (Figure 2b). For the CNN architecture, the X vectors were also grouped consecutively by three and later reformatted, forming a kind of “image” of 3x3 pixels with one channel. (Figure 2c). All training was carried out with 3000 epochs, batch size equal to 64, and a learning rate of

⁴http://mlwiki.org/index.php/ROC_Analysis#ROC_Space

0.0001, using the Keras library from the default configuration of the Google Colab environment. 20% of the 40,000 entries were reserved for testing, while the rest were for training and validation.

5. Model Assessment and Selection (QP1)

5.1. Results on Test Data

About the results for the test data at 10Mbps, both the distribution of the points in the ROC space (Figure 3) and the values in Table 2 point to the good performance of the MLP₁₃ architecture, closely followed by MLP₂₃. In the table, MLP₁₃ architecture performs better in 4 of 5 presented metrics, closely followed by MLP₂₃. In ROC space, the referred models are the ones closest to the top left corner of the graph area. Also noteworthy is the MLP₁₂₃, with performance very close to the models that stood out the most. With accuracy close to 99.5%, LSTM₁₂₃, LSTM₁₃, LSTM₂₃ (with the highest recall) and CNN₁₂₃ models appear to be very promising.

For 100Mbps, the MLP₁₃ and LSTM₁₃ models achieved the highest performance in 4 of 5 metrics, followed by the LSTM₁₂₃ and LSTM₂₃ models. Other models that reached better marks were MLP₁₂₃, CNN₂₃, and MLP₂₃. As seen from the figure 4, all models are very close to the point (0,1) on the respective ROC graph for this scenario.

For the 500Mbps rate, except for models trained only with *ack_ewma* and *send_ewma*, all models presented good results (table 4). The MLP₁₂₃ performed better in 3 of 5 metrics, followed by CNN₁₃ and CNN₂₃, with better accuracy, and F1. These models have the lowest FPR in the ROC space (figure 5). Under the scenario, LSTM₁₃ highlights accuracy. MLP₁₃ and LSTM₂₃ models should also be mentioned, with an error rate below 0.1.

The MLP architecture is the one that stands out the most for 1000Mbps 5, being the one that produced the best results. The models of this architecture are also closer to the upper left corner of the ROC space. LSTM₁₂₃ and CNN₁₂₃ won in Recall, while LSTM₂₃ presented one of the best F1.

The worst performances were due to the models trained with the pair *ack_ewma* and *send_ewma*, with hits below 55%, for 10, 500, and 1000Mbps rates. For 100Mbps, it was below 76%. These models occupy the bottom right corner of all ROC spaces, reaffirming their low performance. The *rtt_ratio* feature is a direct measure of buffer occupancy and, with the others, improves performance. Therefore, the MLP₁₂, LSTM₁₂, and CNN₁₂ models will not be part of the following analyses presented.

Model	Accuracy	Error	Precision	Recall	F1
MLP ₁₂₃	0.997	0.003	0.997	0.998	0.997
MLP ₁₃	0.998	0.002	1.000	0.995	0.998
MLP ₂₃	0.998	0.002	1.000	0.995	0.997
MLP ₁₂	0.547	0.453	0.388	0.582	0.465
LSTM ₁₂₃	0.994	0.006	0.986	1.000	0.993
LSTM ₁₃	0.994	0.006	0.984	1.000	0.992
LSTM ₂₃	0.994	0.006	0.985	1.000	0.992
LSTM ₁₂	0.418	0.582	0.661	0.370	0.475
CNN ₁₂₃	0.994	0.006	0.985	0.999	0.992
CNN ₁₃	0.981	0.019	0.959	0.994	0.976
CNN ₂₃	0.978	0.022	0.950	0.994	0.972
CNN ₁₂	0.502	0.498	0.658	0.419	0.512

Table 2: Test metrics on 10Mbps bottleneck.

Model	Accuracy	Error	Precision	Recall	F1
MLP ₁₂₃	0.998	0.002	0.999	0.996	0.998
MLP ₁₃	0.999	0.001	1.000	0.998	0.999
MLP ₂₃	0.997	0.003	0.999	0.995	0.997
MLP ₁₂	0.571	0.429	0.447	0.589	0.508
LSTM ₁₂₃	0.999	0.001	0.997	1.000	0.998
LSTM ₁₃	0.999	0.001	0.998	0.999	0.999
LSTM ₂₃	0.999	0.001	0.997	0.999	0.998
LSTM ₁₂	0.754	0.246	0.648	0.661	0.654
CNN ₁₂₃	0.998	0.002	0.997	0.998	0.998
CNN ₁₃	0.996	0.004	0.998	0.990	0.994
CNN ₂₃	0.996	0.004	0.999	0.990	0.995
CNN ₁₂	0.746	0.254	0.618	0.655	0.636

Table 3: Test metrics on 100Mbps bottleneck.

Model	Accuracy	Error	Precision	Recall	F1
MLP ₁₂₃	0.912	0.088	0.932	0.894	0.913
MLP ₁₃	0.902	0.098	0.937	0.876	0.906
MLP ₂₃	0.899	0.101	0.911	0.887	0.899
MLP ₁₂	0.652	0.348	0.737	0.629	0.679
LSTM ₁₂₃	0.894	0.106	0.857	0.927	0.891
LSTM ₁₃	0.909	0.091	0.903	0.916	0.909
LSTM ₂₃	0.907	0.093	0.911	0.904	0.908
LSTM ₁₂	0.605	0.395	0.392	0.689	0.500
CNN ₁₂₃	0.890	0.110	0.850	0.925	0.886
CNN ₁₃	0.906	0.094	0.955	0.870	0.911
CNN ₂₃	0.906	0.094	0.954	0.872	0.911
CNN ₁₂	0.603	0.397	0.369	0.699	0.483

Table 4: Test metrics on 500Mbps bottleneck.

Model	Accuracy	Error	Precision	Recall	F1
MLP ₁₂₃	0.8590	0.1410	0.8690	0.8580	0.8630
MLP ₁₃	0.8480	0.1520	0.8650	0.8380	0.8510
MLP ₂₃	0.8480	0.1520	0.8520	0.8360	0.8440
MLP ₁₂	0.5150	0.4850	0.1700	0.5640	0.2610
LSTM ₁₂₃	0.8290	0.1710	0.7880	0.8700	0.8270
LSTM ₁₃	0.8440	0.1560	0.8570	0.8440	0.8510
LSTM ₂₃	0.8230	0.1770	0.7910	0.8560	0.8220
LSTM ₁₂	0.5100	0.4900	0.4090	0.5340	0.4630
CNN ₁₂₃	0.8470	0.1530	0.8370	0.8630	0.8500
CNN ₁₃	0.8420	0.1580	0.8530	0.8430	0.8480
CNN ₂₃	0.8410	0.1590	0.8520	0.8420	0.8470
CNN ₁₂	0.5220	0.4780	0.4460	0.5470	0.4910

Table 5: Test metrics on 1000Mbps bottleneck.

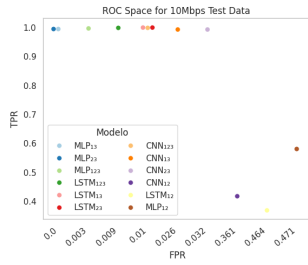


Figure 3: ROC space test Data 10Mbps.

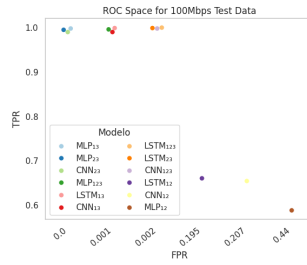


Figure 4: ROC space test Data 100Mbps.

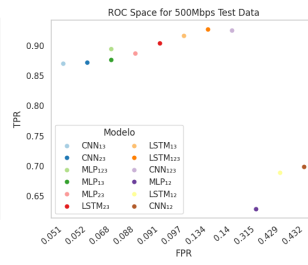


Figure 5: ROC space test Data 500Mbps.

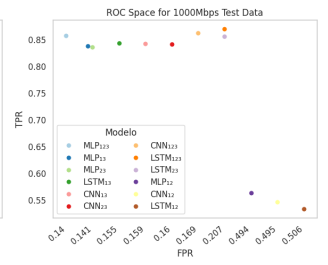


Figure 6: ROC space test Data 1000Mbps.

5.2. Generalization capacity of models (QP1.1, QP1.2, QP 2)

The models had their generalization capacity measured on data from flows that did not participate in the training. To achieve this, new simulations were carried out using the topology in Figure 1, along the same lines as that carried out to collect the training data; however, using different numbers of stations (and their flows) connected to the bottleneck (5, 10, 20, 40) and CC algorithm (NewReno, CUBIC, BBR and Vegas). Since TCP-Vegas did not produce occupancy above 70% on the edge router for 05 flows, there were 15 valid simulations.

After the data preparation processing described previously, each simulation provided a set X of 4000 inputs. Of these 4000 entries, 70% (2,800) were randomly selected, transformed, and classified by each of the 09 surviving models (Section ??). The results, using average values of the metrics, are presented in Table ??:

In general, the models demonstrated excellent generalization capacity. In Table ??, the two values corresponding to the best performance are highlighted in each column, including ties. It can be seen that, again, the MLP_{23} , CNN_{123} and CNN_{13} models stand out. Component 3, rtt_ratio is always present in the best answers.

Model	Accuracy	Error	Precision	Recall	F1
MLP_{123}	0.998	0.002	0.999	0.996	0.998
MLP_{13}	0.997	0.003	0.999	0.996	0.997
MLP_{23}	0.997	0.003	0.999	0.995	0.997
$LSTM_{123}$	0.993	0.007	0.998	0.991	0.994
$LSTM_{13}$	0.993	0.007	0.998	0.990	0.994
$LSTM_{23}$	0.993	0.007	0.998	0.991	0.994
CNN_{123}	0.992	0.008	0.998	0.989	0.994
CNN_{13}	0.963	0.037	0.951	0.983	0.965
CNN_{23}	0.964	0.036	0.952	0.983	0.966

Table 6: Generalization metrics on 10Mbps bnck.

Model	Accuracy	Error	Precision	Recall	F1
MLP_{123}	0.976	0.024	0.991	0.963	0.976
MLP_{13}	0.984	0.016	0.989	0.979	0.984
MLP_{23}	0.973	0.027	0.994	0.955	0.974
$LSTM_{123}$	0.956	0.044	0.981	0.939	0.959
$LSTM_{13}$	0.960	0.040	0.988	0.940	0.963
$LSTM_{23}$	0.956	0.044	0.983	0.937	0.959
CNN_{123}	0.978	0.022	0.992	0.966	0.979
CNN_{13}	0.980	0.020	0.984	0.977	0.980
CNN_{23}	0.980	0.020	0.983	0.979	0.981

Table 7: Generalization metrics on 100Mbps bnck.

Model	Accuracy	Error	Precision	Recall	F1
MLP_{123}	0.970	0.030	0.941	0.998	0.968
MLP_{13}	0.974	0.026	0.950	0.997	0.972
MLP_{23}	0.930	0.070	0.862	0.998	0.922
$LSTM_{123}$	0.967	0.033	0.933	0.999	0.963
$LSTM_{13}$	0.972	0.028	0.943	0.999	0.968
$LSTM_{23}$	0.971	0.029	0.943	0.998	0.968
CNN_{123}	0.968	0.032	0.936	0.998	0.964
CNN_{13}	0.971	0.029	0.945	0.995	0.969
CNN_{23}	0.963	0.037	0.929	0.995	0.960

Table 8: Generalization metrics on 500Mbps bnck.

Model	Accuracy	Error	Precision	Recall	F1
MLP_{123}	0.963	0.037	0.927	1.000	0.958
MLP_{13}	0.974	0.026	0.948	1.000	0.972
MLP_{23}	0.927	0.073	0.853	1.000	0.909
$LSTM_{123}$	0.967	0.033	0.942	0.999	0.969
$LSTM_{13}$	0.974	0.026	0.958	0.996	0.976
$LSTM_{23}$	0.944	0.056	0.902	0.999	0.939
CNN_{123}	0.931	0.069	0.885	0.982	0.918
CNN_{13}	0.955	0.045	0.923	0.996	0.954
CNN_{23}	0.950	0.050	0.915	0.996	0.947

Table 9: Generalization metrics on 1000Mbps bnck.

The models have an impressive performance, as can be seen in the corresponding ROC space (Figure ??), collected from the confusion matrix obtained in each round of classification (each color is a variation of CC and number of flows). The density of points around the position (0,1) and the straight line $TPR=1$ reaffirm the models MLP_{23} (Fig.??), CNN_{123} (Fig. ??) and CNN_{13} (Fig. ??) as the best performers. The CNN_{23} model (Fig. ??) is worth highlighting, with good distribution in the ROC space, however, falling short of the three previously mentioned.

6. Front matter

The author names and affiliations could be formatted in two ways:

- (1) Group the authors per affiliation.
- (2) Use footnotes to indicate the affiliations.

See the front matter of this document for examples. You are recommended to conform your choice to the journal you are submitting to.

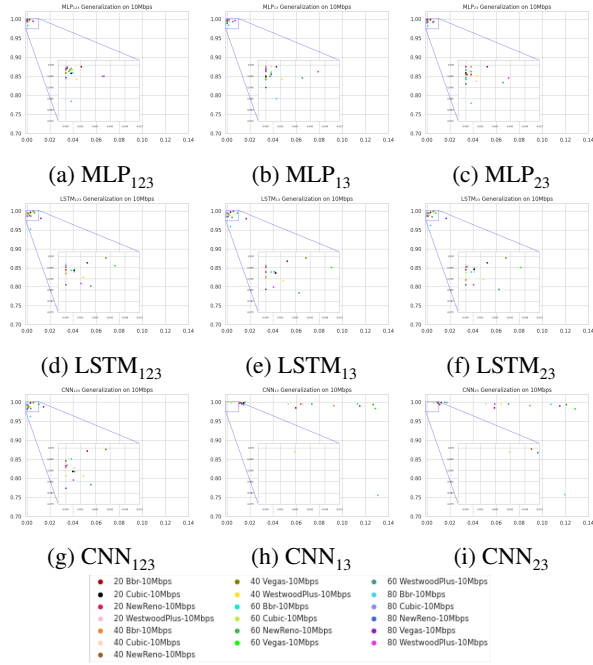


Figure 7: Models generalization capacity, on 10Mbps.

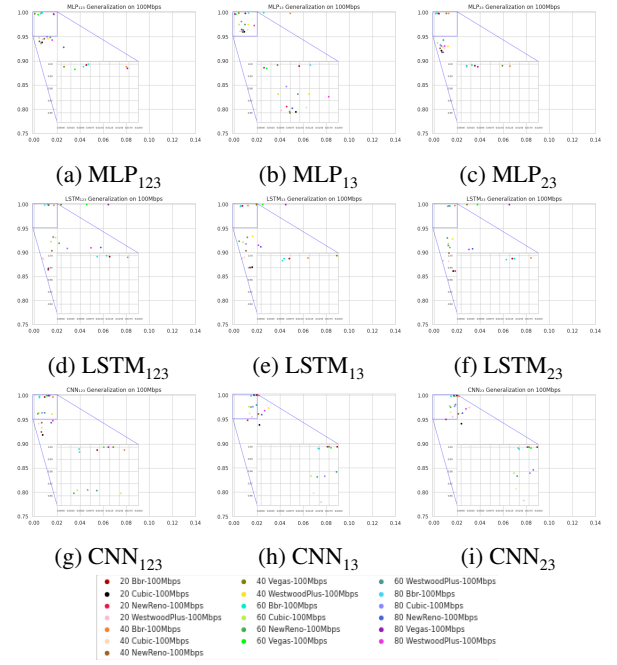


Figure 8: Models generalization capacity, on 100Mbps.

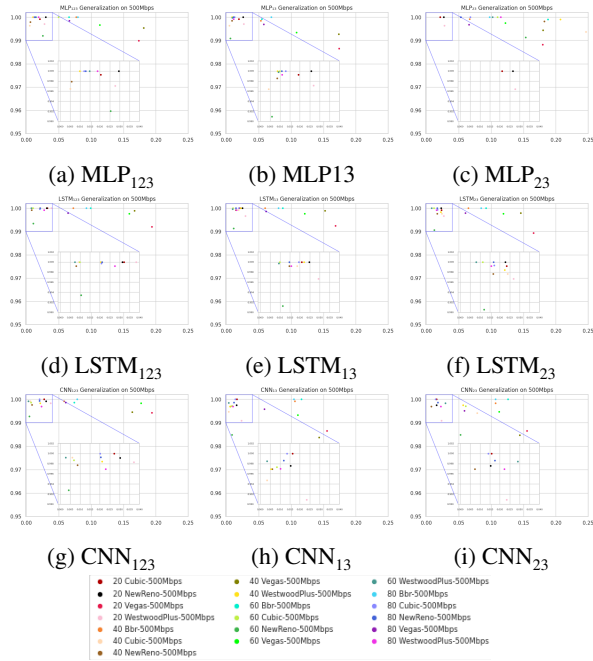


Figure 9: Models generalization capacity, on 500Mbps.

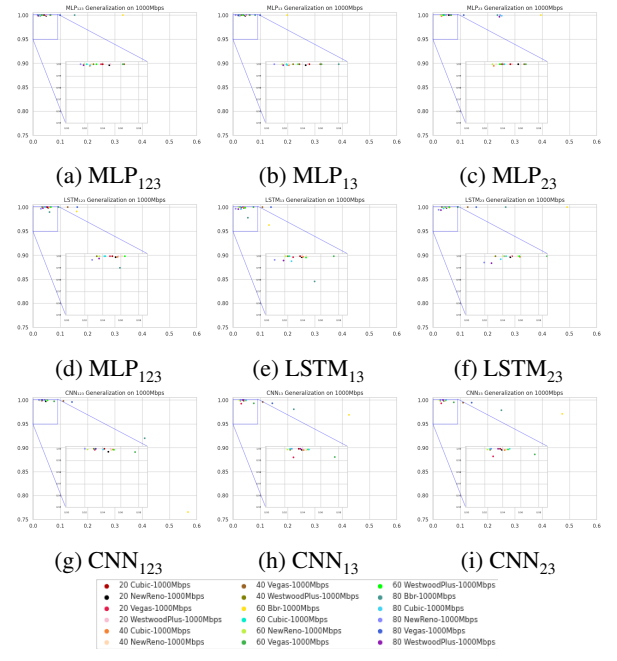


Figure 10: Models generalization capacity, on 1000Mbps.

7. Bibliography styles

There are various bibliography styles available. You can select the style of your choice in the preamble of this document. These styles are Elsevier styles based on standard styles like Harvard and Vancouver. Please use BibTeX to generate your bibliography and include DOIs whenever available.



Figure 11: The beauty of Munnar, Kerala. (See also Table 10).

Here are two sample references: See Fortunato (2010). Also refer Fortunato (2010); Newman and Girvan (2004). More citations are here (Fortunato, 2010; Vehlow, Reinhardt and Weiskopf, 2013).

8. Floats

Figures may be included using the command, `\includegraphics` in combination with or without its several options to further control graphic. `\includegraphics` is provided by `graphic[s,x].sty` which is part of any standard \LaTeX distribution. `graphicx.sty` is loaded by default. \LaTeX accepts figures in the postscript format while pdf\LaTeX accepts *.pdf, *.mps (metapost), *.jpg and *.png formats. pdf\LaTeX does not accept graphic files in the postscript format.

The `table` environment is handy for marking up tabular material. If users want to use `multirow.sty`, `array.sty`, etc., to fine control/enhance the tables, they are welcome to load any package of their choice and `cas-sc.cls` will work in combination with all loaded packages.

Table 10

This is a test caption. This is a test caption. This is a test caption. This is a test caption.

Col 1	Col 2	Col 3	Col4
12345	12345	123	12345
12345	12345	123	12345
12345	12345	123	12345
12345	12345	123	12345
12345	12345	123	12345

9. Theorem and theorem like environments

`cas-sc.cls` provides a few shortcuts to format theorems and theorem-like environments with ease. In all commands the options that are used with the `\newtheorem` command will work exactly in the same manner. `cas-sc.cls` provides three commands to format theorem or theorem-like environments:

```

\newtheorem{theorem}{Theorem}
\newtheorem{lemma}[theorem]{Lemma}
\newdefinition{rmk}{Remark}
\newproof{pf}{Proof}
\newproof{pot}{Proof of Theorem \ref{thm2}}

```

The `\newtheorem` command formats a theorem in L^AT_EX's default style with italicized font, bold font for theorem heading and theorem number at the right hand side of the theorem heading. It also optionally accepts an argument which will be printed as an extra heading in parentheses.

```

\begin{theorem}
  For system (8), consensus can be achieved with
   $\|T_{\omega z}\| \dots$ 
  \begin{eqnarray}\label{10}
    \dots
  \end{eqnarray}
\end{theorem}

```

Theorem 1. *For system (8), consensus can be achieved with $\|T_{\omega z}\| \dots$*

(1)

The `\newdefinition` command is the same in all respects as its `\newtheorem` counterpart except that the font shape is roman instead of italic. Both `\newdefinition` and `\newtheorem` commands automatically define counters for the environments defined.

The `\newproof` command defines proof environments with upright font shape. No counters are defined.

10. Enumerated and Itemized Lists

cas-sc.cls provides an extended list processing macros which makes the usage a bit more user friendly than the default L^AT_EX list macros. With an optional argument to the `\begin{enumerate}` command, you can change the list counter type and its attributes.

```

\begin{enumerate}[1.]
\item The enumerate environment starts with an optional
  argument '1.', so that the item counter will be suffixed
  by a period.
\item You can use 'a' for alphabetical counter and '(i)' for
  roman counter.
\begin{enumerate}[a]
  \item Another level of list with alphabetical counter.
  \item One more item before we start another.
  \item One more item before we start another.
  \item One more item before we start another.
  \item One more item before we start another.
\end{enumerate}
\end{enumerate}

```

Further, the enhanced list environment allows one to prefix a string like 'step' to all the item numbers.

```

\begin{enumerate}[Step 1.]
\item This is the first step of the example list.
\item Obviously this is the second step.
\item The final step to wind up this example.
\end{enumerate}

```

11. Cross-references

In electronic publications, articles may be internally hyperlinked. Hyperlinks are generated from proper cross-references in the article. For example, the words Fig. 1 will never be more than simple text, whereas the proper cross-reference `\ref{tiger}` may be turned into a hyperlink to the figure itself: Fig. 1. In the same way, the words Ref. [1] will fail to turn into a hyperlink; the proper cross-reference is `\cite{Knuth96}`. Cross-referencing is possible in \LaTeX for sections, subsections, formulae, figures, tables, and literature references.

12. Bibliography

Two bibliographic style files (*.bst) are provided — `modell-num-names.bst` and `model2-names.bst` — the first one can be used for the numbered scheme. This can also be used for the numbered with new options of `natbib.sty`. The second one is for the author year scheme. When you use `model2-names.bst`, the citation commands will be like `\citep`, `\citet`, `\citealt` etc. However when you use `modell-num-names.bst`, you may use only `\cite` command.

the `thebibliography` environment. Each reference is a `\bibitem` and each `\bibitem` is identified by a label, by which it can be cited in the text:

In connection with cross-referencing and possible future hyperlinking it is not a good idea to collect more than one literature item in one `\bibitem`. The so-called Harvard or author-year style of referencing is enabled by the \LaTeX package `natbib`. With this package the literature can be cited as follows:

- Parenthetical: `\citep{WB96}` produces (Wettig & Brown, 1996).
- Textual: `\citet{ESG96}` produces Elson et al. (1996).
- An affix and part of a reference: `\citep[e.g.]{Ch. 2}{Gea97}` produces (e.g. Governato et al., 1997, Ch. 2).

In the numbered scheme of citation, `\cite{<label>}` is used, since `\citep` or `\citet` has no relevance in the numbered scheme. `natbib` package is loaded by `cas-sc` with numbers as default option. You can change this to author-year or harvard scheme by adding option `authoryear` in the class loading command. If you want to use more options of the `natbib` package, you can do so with the `\biboptions` command. For details of various options of the `natbib` package, please take a look at the `natbib` documentation, which is part of any standard \LaTeX installation.

A. My Appendix

Appendix sections are coded under `\appendix`.

`\printcredits` command is used after appendix sections to list author credit taxonomy contribution roles tagged using `\credit` in frontmatter.

CRedit authorship contribution statement

J.K. Krishnan: Conceptualization of this study, Methodology, Software. **William J. Hansen:** Data curation, Writing - Original draft preparation.

References

- Fortunato, S., 2010. Community detection in graphs. *Phys. Rep.-Rev. Sec. Phys. Lett.* 486, 75–174.
- Fukushima, K., 1980. Neocognitron: A self-organizing neural network model for a mechanism of pattern recognition unaffected by shift in position. *Biological Cybernetics* 36, 193–202. URL: <https://doi.org/10.1007/BF00344251>, doi:10.1007/BF00344251. 0000061.
- Hochreiter, S., Schmidhuber, J., 1997. Long Short-Term Memory. *Neural Computation* 9, 1735–1780. URL: <https://ieeexplore.ieee.org/abstract/document/6795963>, doi:10.1162/neco.1997.9.8.1735. 0000060 Conference Name: Neural Computation.
- ITU, G.C.R., 2023. Global Connectivity Report 2022 - <https://www.itu.int/itu-d/reports/statistics/2022/05/29/gcr-chapter-1> acesso em 13/12/23. URL: <https://www.itu.int/itu-d/reports/statistics/2022/05/29/gcr-chapter-1>.
- Lippmann, R., 1987. An introduction to computing with neural nets. *IEEE ASSP Magazine* 4, 4–22. URL: <https://ieeexplore.ieee.org/document/1165576>, doi:10.1109/MASSP.1987.1165576. 0000062 Conference Name: IEEE ASSP Magazine.
- Newman, M.E.J., Girvan, M., 2004. Finding and evaluating community structure in networks. *Phys. Rev. E* 69, 026113.
- ns3, 2023. A discrete-event network simulator for internet systems - <https://www.nsnam.org> - vistado em 13/12/05.
- Vehlow, C., Reinhardt, T., Weiskopf, D., 2013. Visualizing fuzzy overlapping communities in networks. *IEEE Trans. Vis. Comput. Graph.* 19, 2486–2495.

[illegible][illegible][illegible]